DFT Computational Study of the Mechanism of Allyl Chloride Carbonylation Catalyzed by Palladium Complexes

M. Angels Carvajal,[†] Gian Pietro Miscione,[‡] Juan J. Novoa,*[,†] and Andrea Bottoni*[,‡]

Dipartimento di Chimica "G. Ciamician", Università di Bologna, via Selmi 2, 40126 Bologna, Italy, and Department de Quimica Fisica, Facultat de Quimica, and CERQT, Park Cientific, Universitat de Barcelona, Av. Diagonal 647, 08028-Barcelona, Spain

Received September 8, 2004

A theoretical DFT (B3LYP) investigation on the carbonylation reaction of allyl chloride catalyzed by $Cl_2Pd(PH_3)_2$ is discussed. The computational results show the following. (i) The favored reaction channel leading to the β,γ-unsaturated acyl chloride product is a direct attack of the chlorine atom on the metal (σ pathway). (ii) The carbonylation pathway involving the formation of π-allyl complexes is highly disfavored. (iii) In the π complexes the ligand is not η^3-coordinated to the metal, as usually assumed, but η^2-coordinated. (iv) The presence of a favored σ pathway seems to be a common feature of this class of reactions (i.e. metal-catalyzed carbonylation of allyl halides). (v) The $Cl_2Pd(CO)_2$ complex, which forms from $Cl_2Pd(PH_3)_2$, can behave as an "active" catalytic species. In the presence of high CO pressures, it initiates an alternative pathway that can be competitive with the main σ pathway.

Introduction

The carbonylation of allylic substrates catalyzed by transition-metal complexes offers a valuable synthetic tool to obtain β,γ-unsaturated carboxylic acid derivatives.[1] The use of different transition-metal complexes as catalysts is well documented in a number of papers available in the literature.[1−16] The carbonylation of allyl chlorides, catalyzed by nickel tetracarbonyl, was reported for the first time by Chiusoli.[2] A few years later Heck confirmed the nature of the product of this reaction and discussed possible reaction mechanisms.[3] Even if this reaction proceeds under mild conditions (room temperature and atmospheric pressure), it has a disadvantage in that a large amount of nickel tetracarbonyl must be used (more than 0.5 mol of nickel carbonyl/mol of allyl chloride). Furthermore, the direct manipulation of $Ni(CO)_4$ is difficult because of the high toxicity of this species. For these reasons palladium complexes have extensively replaced nickel complexes as catalytic species in these reactions.

One of the first examples of palladium-catalyzed carbonylation of allyl chlorides was carried out by Long and co-workers[4] during the 1960s. They demonstrated that, when allylic chlorides are heated under pressure with carbon monoxide in the presence of small quantities of π-allylic palladium chloride complexes, alk-3-enoyl chlorides are formed. They also discovered that the reaction is catalyzed by palladium chloride ($PdCl_2$) and even metallic palladium. At the same time the reaction of allyl chloride and allyl alcohol with carbon monoxide in ethanol catalyzed by $PdCl_2$ was carefully examined by Tsuji et al.[5] They found that the main product of the reaction is ethyl 3-butenoate and that other allylic compounds (allylic esters and ethers) react in the same way. However, this reaction, although synthetically useful, has some disadvantages. It requires high CO pressure and high temperature, is very slow, and results in modest yields of carbonylation products. Thus, various methods and alternative synthetic procedures have been proposed during the last three decades for a low-pressure and low-temperature route to carbonylation. For instance, Milstein found that in the presence of carboxylic acid anions the carbonylation of (π-allyl)palladium complexes can be accomplished quantitatively at low pressure and temperature.[6] A smooth palladium-catalyzed carbonylation has been reported by Tsuji and co-workers[7] for allylic carbonates and by Murahashi and co-workers[9] for allyl phosphates

* To whom correspondence should be addressed. E-mail: andrea.bottoni@unibo.it (A.B.); novoa@qf.ub.es (J.J.N.).
† Università di Bologna.
‡ Universitat de Barcelona.

(1) Yamamoto, A. *Bull. Chem. Soc. Jpn*. **1995**, *68*, 433 and references therein.
(2) Chiusoli, G. P. *Chim. Ind.* **1959**, *41*, 503. Chiusoli, G. P. *Angew. Chem*. **1960**, *72*, 74. Chiusoli, G. P.; Cassar, L. *Angew. Chem., Int. Ed. Engl*. **1967**, *6*, 124.
(3) Heck, R. F. *J. Am. Chem. Soc.* **1963**, *85*, 2013.
(4) Dent, W. T.; Long, R.; Whitfield, G. H. *J. Chem. Soc*. **1964**, 1588. Long, R.; Whitfield, G. H. *J. Chem. Soc*. **1964**, 1852.
(5) Tsuji, J.; Kiji, J.; Imamura, S.; Morikawa, M. *J. Am. Chem. Soc.* **1964**, *86*, 4350. Tsuji, J. *Acc. Chem. Res.* **1969**, *2*, 144.
(6) Mllstein, D. *Organometallics* **1982**, *1*, 888.
(7) Tsuji, J.; Sato, K.; Okumoto, H. *J. Org. Chem.* **1984**, *49*, 1341.
(8) Kiji, J.; Okano, T.; Ono, I.; Konoishi, H. *J. Mol. Catal*. **1987**, *39*, 355.
(9) Murahashi, S.-I.; Imada, Y.; Taniguchi, Y.; Higashiura, S. *Tetrahedron Lett*. **1988**, *29*, 4945.
(10) Okano, T.; Okabe, N. *Bull. Chem. Soc. Jpn*. **1992**, *65*, 2589.
(11) Kiji, J.; Okano, T.; Higashimae, Y.; Fukui, Y. *Bull. Chem. Soc. Jpn*. **1996**, *69*, 1029.
(12) Jiang, H.; Xu, Y.; Liao, S.; Yu, D.; Chen, H.; Li, X. *J. Mol. Catal.* **1998**, *130*, 79.
(13) Bertoux, F.; Monflier, E.; Castanet, Y.; Montreux, A. *J. Mol. Catal.* **1999**, *143*, 11.
(14) El Houssame, S.; El Firdoussi, L.; Allaoud, S.; Karim, A.; Castanet, Y.; Mortreux, A. *J. Mol. Catal. A: Chem.* **2001**, *168*, 15.
(15) Knight, J. G.; Tchabanenko, K. *Tetrahedron* **2002**, *58*, 6659.
(16) Song, R.; Zeng, J.; Zhong, B. *Catal. Lett*. **2002**, *82*, 89.

10.1021/om049301y CCC: $30.25 © 2005 American Chemical Society
Publication on Web 03/24/2005

Scheme 1

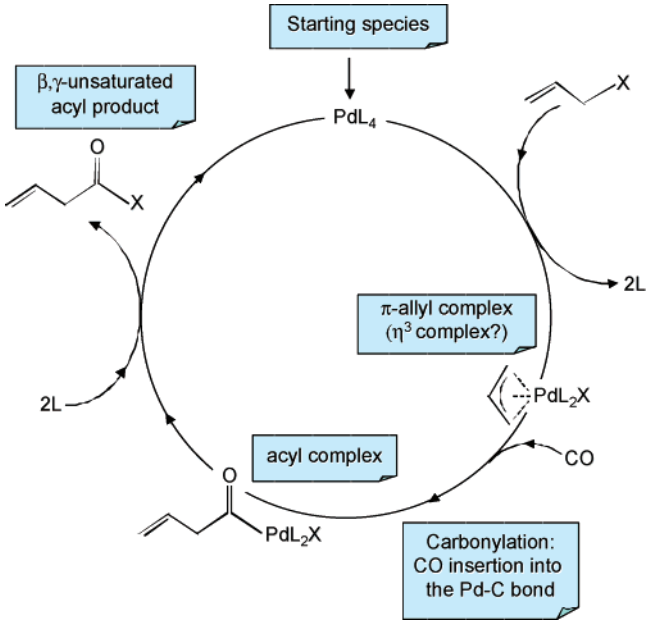

and allyl acetates. Several workers have further improved the palladium-catalyzed carbonylation of allylic systems using different reaction conditions and different palladium complexes. For instance, Okano and Okabe[10] have established a synthetic route for a palladium-catalyzed carbonylation of allylic halides under atmospheric pressure. The process proceeds readily in an aqueous sodium hydroxide/organic solvents two-phase system using a palladium phosphine complex such as $Cl_2Pd(PPh_3)_2$ or the phosphine-free complex disodium tetrachloropalladate complex, $Na_2(PdCl_4)$. During the last few years other authors have suggested various synthetic procedures for carbonylation reactions in one-phase or two-phase systems.[11−15] Recently, a palladium-catalyzed alkoxycarbonylation of allyl bromide to unsaturated esters has been performed by Song and coworkers in supercritical carbon dioxide.[16]

The formation of a π-allyl palladium intermediate (η^3 complex) is postulated in the commonly accepted mechanism of palladium-catalyzed carbonylation reactions. A possible catalytic scheme based on this hypothesis and involving the tetracoordinated palladium complex PdL_4 (such as $Cl_2Pd(PPh_3)_2$) is shown in Scheme 1. After the π-allyl palladium complex is formed, CO inserts into a carbon−palladium bond, leading to a palladium β,γ-unsaturated acyl complex. This complex, after release of the product, again forms the catalytic species and enters a new catalytic cycle. This mechanism is similar to that proposed for the carbonylation of allyl halide catalyzed by nickel carbonyl which we have very recently investigated. In that case we carried out a DFT theoretical investigation of the carbonylation reaction of allyl bromide catalyzed by nickel tetracarbonyl, $Ni(CO)_4$,[17] and found that in addition to the π pathway (involving η^3 complexes) shown in Scheme 1, an alternative path (σ pathway) exists. This corresponds to a direct attack of the halogen on the metal (leading to a η^1-allyl−$Ni(CO)_3Br$ complex) and is the energetically most favored one.

A catalytic scheme similar to that found for $Ni(CO)_4$ could apply, in principle, to carbonylation reactions of allylic systems catalyzed by palladium complexes. To elucidate this aspect and other points that are still obscure (nature of the catalytic active species, structure of the complex intermediates, rate-determining step of the process), we have investigated at the DFT level the carbonylation of allyl systems catalyzed by palladium complexes. This has been done in a systematic way, specifically including the possibility of π and σ pathways. As far as we know, no accurate quantum-mechanical studies addressing these points for this particular reacting system are available in the literature, even if various theoretical investigations on transition-metal-catalyzed carbonylations are reported.[18−20] The model system that we have chosen here is formed by allyl choride reacting with CO in the presence of a $Cl_2Pd(PH_3)_2$ complex. This complex emulates the catalytic behavior of $Cl_2Pd(PPh_3)_2$, one of the most effective and widely used palladium-based catalysts.[15] In addition to $Cl_2Pd(PH_3)_2$, we have also considered as possible active catalytic species the complexes $Cl_2Pd(CO)PH_3$ and $Cl_2Pd(CO)_2$, which could be formed in the reaction mixture in the presence of carbon oxide.

An important aspect, concerning the palladium oxidation state of the active catalytic complex, should be briefly noted. Our model system clearly emulates a Pd(II) catalytic species, even if the conversion of the starting Pd(II) complexes to Pd(0) species is often postulated. However, there is no evidence that this process occurs no matter what the reaction conditions. When $Cl_2Pd(PR_3)_2$ complexes are used as a source of Pd(0) species, the addition of a reducer[21] or the application of electrochemical techniques[22] are required. Also, there is evidence that some Pd(II) salts are reduced by phosphines only in the presence of oxygenated ligands or oxygenated substances in the reaction medium.[23] In many cases the oxidation state of the active catalyst is not well established and many examples are reported, supporting the idea that the real catalyst is either a Pd(II) species or a Pd(0) intermediate.[24−27]

In particular, many examples pointing to a Pd(II) species can be provided. Some Pd catalysts, for instance, in the absence of a suitable stabilizer, are deactivated since they tend to decompose to Pd black or to form dinuclear complexes.[24] Since the activity of a catalyst can be restored by means of an acid treatment, the acid HX is believed to stabilize Pd in the active divalent state as PdX_2 species.[25−27] While in several papers it has been reported that $Pd(PPh_3)_4$ behaves as an active catalyst, in contrast to this result, $Pd(PPh_3)_4$ has been demonstrated to reduce the activity of $Cl_2Pd(PPh_3)_2/10PPh_3$ in the hydroesterification of styrene.[24] Also, it has been

(17) Bottoni, A.; Miscione, G. P.; Novoa, J. J.; Prat-Resina, X. *J. Am. Chem. Soc*. **2003**, *125*, 10412.

(18) Carbo, J. J.; Bo, C.; Poblet, J. M.; Moreto, J. M. *Organometallics* **2000**, *19*, 3516.
(19) Cavallo, L.; Sola, M. *J. Am. Chem. Soc*. **2001**, *123*, 12294.
(20) Daura-Oller, E.; Poblet, J. M.; Bo, C. *Dalton* **2003**, 92.
(21) Neghishi, E.-I.; King, A. O.; Okukado, N. *J. Org. Chem.* **1977**, *42*, 1821. Fauvarque, J. F.; Jutand, A. *Bull. Soc. Chim. Fr.* **1976**, 765.
(22) Amatore, C.; Azzabi, M.; Jutand, A. *J. Organomet. Chem.* **1989**, *363*, C41.
(23) Amatore, C.; Jutand, A. *J. Organomet. Chem.* **1999**, *576*, 254.
(24) Kiss, G. *Chem. Rev.* **2001**, *101*, 3435 and refs 13k,q,s, 14b, 20f, and 49 therein.
(25) Knifton, J. F. *J. Am. Oil Chem. Soc.* **1978**, *55*, 496.
(26) Fenton, D. M. *J. Org. Chem.* **1973**, *38*, 3192.
(27) Bittler, K.; Kutepow, N.; Neubauer, D.; Reis, H. *Angew. Chem., Int. Ed. Engl.* **1968**, *7*, 329.

suggested by Bittler and co-workers[27] that Pd(0) complexes are not active unless HCl is added to the reaction mixture. Further experimental evidence pointing to the involvement of Pd(II) species in the catalytic cycle is the fact that the nature of the counterion can significantly affect both the rate and the selectivity of the reaction.[24]

Another interesting point that should be stressed is the evidence that the addition of phosphines increases the catalytic activity. It is believed that this effect is due to the stabilization of the catalytic species. However, since phosphines can complex both Pd(0) and Pd(II), this stabilization can be effective in both oxidation states.[24]

Thus, it is evident from the literature that the nature of the real catalyst and, in particular, its oxidation state is still obscure and is subject to debate. Probably, either species (Pd(0) or Pd(II)) can act as a true catalyst, depending on the reaction conditions and the nature of the precatalyst complex. In the present paper we have chosen to investigate the case of a Pd(II) species acting as a catalyst, which seems to be a likely hypothesis when $Cl_2Pd(PPh_3)_2$ complexes are used in the absence of additional substances (suitable reducer or oxygenated ligands) in the reaction medium.

Computational Procedures

All the DFT computations reported here have been performed with the Gaussian 98[28] series of programs using the nonlocal hybrid Becke three-parameter exchange functional,[29,30] denoted as B3LYP. This functional has been demonstrated to provide a reliable description (structures and energies) of transition-metal complexes and of the potential surfaces associated with catalytic processes.[17,31,32] The geometry of the various critical points on the reaction surface has been fully optimized with the gradient method available in Gaussian 98 using two different basis sets: (i) the all-electron DZVP basis,[33] which is a local spin density (LSD) optimized basis set of double-ζ quality in the valence shell plus polarization functions and (ii) a basis formed by the energy-adjusted pseudopotential basis set proposed by Preuss and co-workers[34] (denoted as sdd pseudopotentials in the Gaussian 98 formalism) for the metal and by the 6-31G* basis[28] for the remaining atoms. This basis is denoted here as the sdd/6-31G* basis. In the following sections only the results obtained with the more extended basis (sdd/6-31G*) will be discussed in detail. These results will be briefly compared to the DZVP results in a final section. To roughly evaluate the effect of the solvent, we carried out single-point computations on the most important gas-phase optimized structures (reactants and more energetic transitions states) using the polarized continuous model (PCM)[35] method available in Gaussian 98.

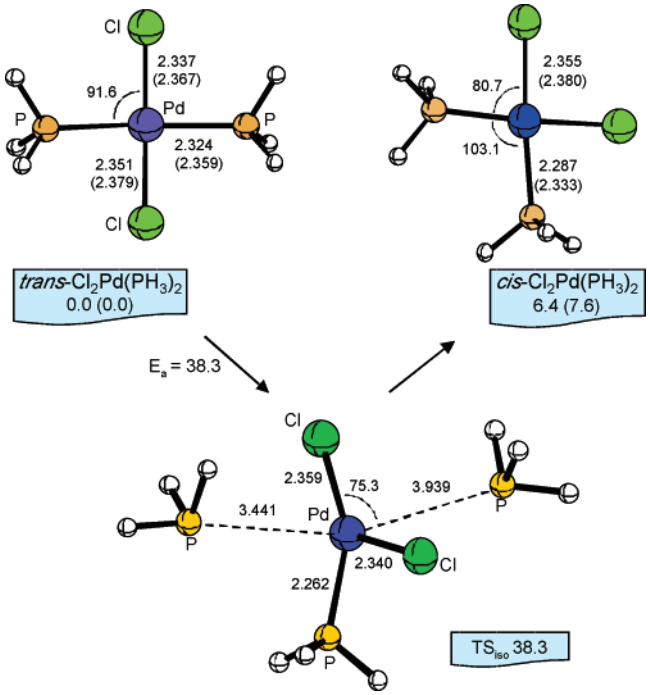

Figure 1. Schematic representation of the trans and cis isomers of $Cl_2Pd(PH_3)_2$ and isomerization transition state (TS_{iso}). The energies (kcal mol^{-1}) are relative to the trans species. E_a = activation barriers. Values in parentheses: DZVP basis. Bond lengths in angstroms and angles in degrees.

Results and Discussion

In this section we first discuss the singlet potential energy surface associated with the reaction of the allyl chloride substrate with CO and $Cl_2Pd(PH_3)_2$. In addition to the $Cl_2Pd(PH_3)_2$ complex, we also consider $Cl_2Pd(CO)PH_3$ and $Cl_2Pd(CO)_2$ as possible active catalytic species. These two complexes are likely to form under the real experimental conditions and especially when an excess of CO is used.

A. Reaction with $Cl_2Pd(PH_3)_2$: Formation of π-η^2-Allyl Palladium Complexes. The $Cl_2Pd(PH_3)_2$ complex can exist as two isomers, a trans and a cis isomer (Figure 1), the former being 6.4 kcal mol^{-1} more stable than the latter. The higher energy of the cis species is probably due to the repulsion between the two adjacent phosphine groups, which results in a value of the $\angle$P−Pd−P angle larger than 90° (103.1°). We could not find a transition state for the trans → cis isomerization, since one of the two PH_3 groups of $Cl_2Pd(PH_3)_2$ detaches from the metal during this structural transformation. However, we found that the isomerization becomes possible when a third phosphine ligand is involved (see Figure 1). The new PH_3 enters the metal coordination sphere and determines the expulsion of one of the two PH_3 groups attached to the Pd atom by overcoming a barrier of 38.3 kcal mol^{-1}. It is interesting

(28) Frisch, M. J.; Trucks, G. W.; Schlegel, H. B.; Scuseria, G. E.; Robb, M. A.; Cheeseman, J. R.; Zakrzewski, V. G.; Montgomery, J. A., Jr.; Stratmann, R. E.; Burant, J. C.; Dapprich, S.; Millam, J. M.; Daniels, A. D.; Kudin, K. N.; Strain, M. C.; Farkas, O.; Tomasi, J.; Barone, V.; Cossi, M.; Cammi, R.; Mennucci, B.; Pomelli, C.; Adamo, C.; Clifford, S.; Ochterski, J.; Petersson, G. A.; Ayala, P. Y.; Cui, Q.; Morokuma, K.; Malick, D. K.; Rabuck, A. D.; Raghavachari, K.; Foresman, J. B.; Cioslowski, J.; Ortiz, J. V.; Stefanov, B. B.; Liu, G.; Liashenko, A.; Piskorz, P.; Komaromi, I.; Gomperts, R.; Martin, R. L.; Fox, D. J.; Keith, T.; Al-Laham, M. A.; Peng, C. Y.; Nanayakkara, A.; Gonzalez, C.; Challacombe, M.; Gill, P. M. W.; Johnson, B. G.; Chen, W.; Wong, M. W.; Andres, J. L.; Head-Gordon, M.; Replogle, E. S.; Pople, J. A. *Gaussian 98*, revision A.6; Gaussian, Inc.: Pittsburgh, PA, 1998.

(29) Becke, A. D. *J. Chem. Phys.* **1993**, *98*, 1372, 5648.

(30) Stephens, P. J.; Devlin, F. J.; Chabalowsky, C. F.; Frisch, M. J. *J. Phys. Chem.* **1994**, *98*, 11623.

(31) Bottoni, A.; Perez Higueruelo, A.; Miscione, G. P. *J. Am. Chem. Soc.* **2002**, *124*, 5506.

(32) De Angelis, F.; Sgamellotti, A. *Organometallics* **2000**, *19*, 4104.

(33) Godbout, N.; Salahub, D. R.; Andzelm, J.; Wimmer, E. *Can. J. Chem.* **1992**, *70*, 560. UniChem DGauss, Version 2.3.1; Cray Research, Inc., 1994.

(34) Andrade, D.; Haeussermann, U.; Dolg, M.; Stoll, H.; Preuss, H. *Theor. Chim. Acta* **1990**, *77*, 123.

(35) Miertus, S.; Scrocco, E.; Tomasi, J. *J. Chem. Phys.* **1981**, *55*, 117. Miertus, S.; Tomasi, J. *J. Chem. Phys.* **1982**, *65*, 239.

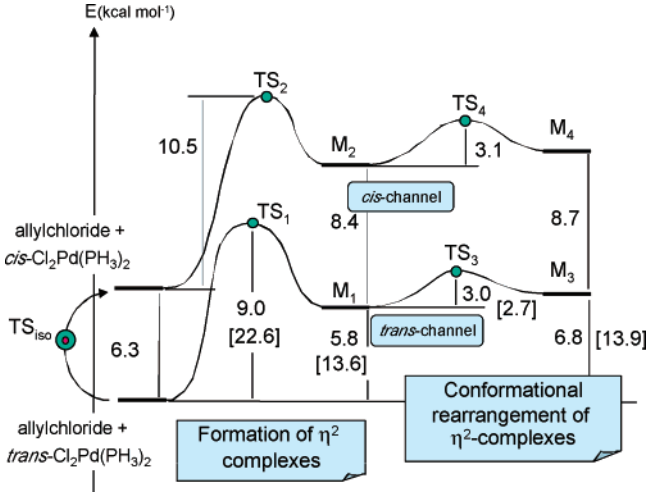

Figure 2. Energy profiles corresponding to the formation of η^2 complexes (energy values in kcal mol^{-1}). Values in brackets include solvent effects (sdd/6-31G* basis).

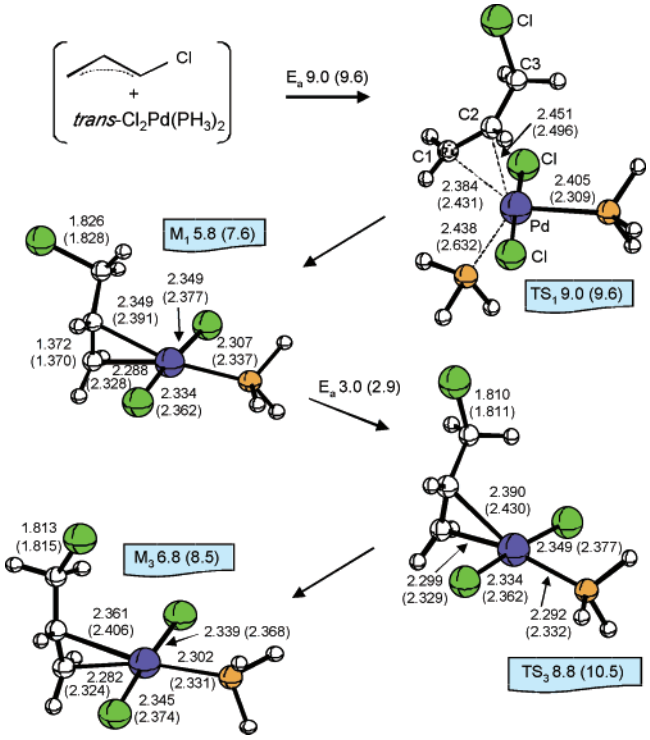

Figure 3. Schematic representation of the structures of M_1, TS_1, TS_3, and M_3. The energies (kcal mol^{-1}) are relative to noninteracting *trans*-$Cl_2Pd(PH_3)_2$ and allyl chloride (asymptotic limit). E_a = activation barriers. Values in parentheses: DZVP basis. The absolute energy of the asymptotic limit is −2425.525 368 au (sdd/6-31G* basis) and −7237.198 999 au (DZVP basis). Bond lengths are in angstroms and angles in degrees.

to notice that in the corresponding transition state (TS_{iso}) the two phosphorus atoms and the palladium are not collinear (the ∠PPdP angle is 154.3°) and the two chlorine atoms are not equivalent (the Pd−Cl distances are 2.359 and 2.340 Å). The metal has a trigonal-planar structure with one PH_3 and two Cl ligands lying on the same plane.

The two energy profiles for the reaction of the substrate molecule with either the trans or cis form of $Cl_2Pd(PH_3)_2$ are represented in Figure 2 (trans and cis channels), while the structures of the critical points located on the two potential surfaces are reported in Figure 3 (trans isomer) and Figure 4 (cis isomer). For both species we have observed the formation of a preliminary π η^2 complex (M_1 and M_2 along the two channels), where the terminal CC double bond of the substrate interacts with the palladium atom. The corresponding transition states are TS_1 (trans) and TS_2 (cis). Here the substrate that attacks the Pd atom causes the expulsion of one PH_3 ligand from the metal coordination sphere. M_1 is 5.8 kcal mol^{-1} higher than the asymptotic limit (i.e. the $Cl_2Pd(PH_3)_2$ complex and the noninteracting allyl chloride substrate) and 8.4 kcal mol^{-1} more stable than M_2. The activation energies required to form the new allyl palladium complexes are 9.0 (trans) and 10.5 kcal mol^{-1} (cis). The two η^2 complexes have rather similar structural features. In both cases the orientation of the chlorine atom is anti to the metal and the C1−C2 bond has slightly lost its double-bond character (1.372 and 1.383 Å are the C1−C2 bond lengths in M_1 and M_2, respectively, to be compared to 1.334 Å in the allyl chloride reactant) because the π system is now interacting with the metal. A slight trans effect due to the phosphine ligand can be seen in the change of the Pd−C bond lengths on passing from M_1 to M_2: these bonds vary from 2.349 and 2.228 Å (M_1) to 2.274 and 2.231 Å (M_2). The two η^2 complexes can undergo a conformational rearrangement, which is basically a rotation around the C2−C3 bond of the allyl moiety. This requires overcoming a barrier of 3.0 kcal mol^{-1} along the trans channel (transition state TS_3) and 3.1 kcal mol^{-1} along the cis channel (transition state TS_4). This rotation leads to M_3 (trans) and M_4 (cis), which are slightly higher in energy than M_1 and M_2, respectively, and where the chlorine atom is approximately syn to the metal.

Finally, it is important to note that, despite exhaustive explorations, we have not found any intermediate where the ligand is η^3 coordinated to the metal. Thus, we can discard the existence of a low-energy pathway of such a type with the catalytic species considered here.

B. The Carbonylation Step: From the η^2 Complexes to the Acyl Product. The two pathways leading from the η^2 complexes (M_4 and M_3) to the final acyl products involve complex molecular transformations. We first examine in detail the lower energy path (trans channel) originating from the trans species (M_3). The corresponding energy profile is reported in Figure 5 together with that of the cis channel. The structures of the various critical points of the trans channel are depicted in Figures 6 and 7. Since the structures of the points found along the cis channel are very similar, we have moved them into the Supporting Information (Figures 1S and 2S).

To describe the carbonylation process, we have considered a CO molecule approaching M_3. Surprisingly, the formation of the acyl product does not take place by direct insertion of CO into the Pd−C bond or by CO addition to the metal. Instead, the approaching CO simultaneously interacts with one of the two chlorine ligands and with the terminal carbon of the allyl chloride double bond (Figure 6), causing the rupture of the Pd−C bond. This is evident in transition state TS_5, where the breaking Pd−C bond is 3.031 Å and the distances C(CO)−C(allyl chloride) and C(CO)−Cl are

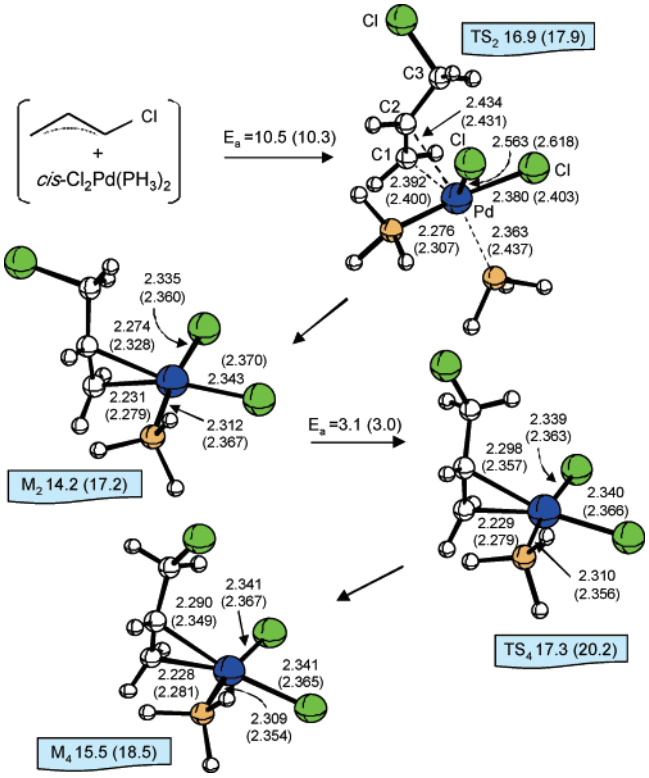

Figure 4. Schematic representation of the structures of TS_2, M_2, TS_4, and M_4. The energies (kcal mol^{-1}) are relative to noninteracting *trans*-$Cl_2Pd(PH_3)_2$ and allyl chloride (asymptotic limit). E_a = activation barriers. Values in parentheses: DZVP basis. Bond lengths are in angstroms and angles in degrees.

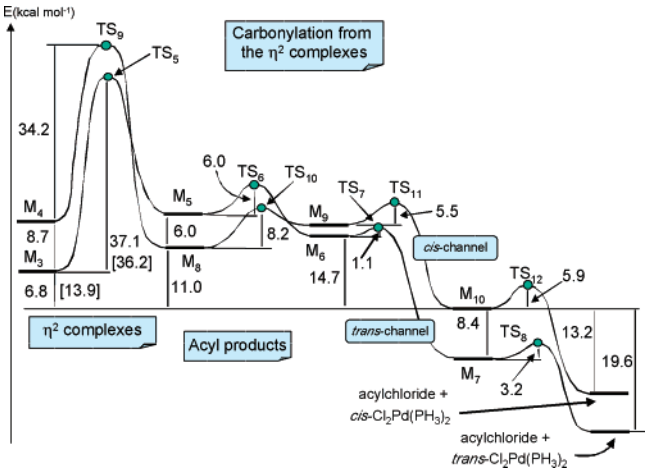

Figure 5. Energy profiles corresponding to the carbonylation from η^2 complexes (energy values in kcal mol^{-1}). Values in brackets include solvent effects (sdd/6-31G* basis).

2.023 and 2.540 Å, respectively. TS_5 has a large activation energy (37.1 kcal mol^{-1}) and leads to a new intermediate (M_5) characterized by a cyclic pentaatomic structure including palladium and one chlorine ligand. This chlorine atom is bridging the metal and the carbon of the carbonyl group. As a consequence, here the Cl−Pd bond is longer (2.431 Å) than in the η^2 complex.

To obtain a free acyl chloride group, the chlorine of the substrate attacks the metal and determines the expulsion of the bridged Cl from the metal coordination sphere ($M_5 \rightarrow M_6$). This transformation requires overcoming a small barrier (6.0 kcal mol^{-1}, corresponding to transition state TS_6), where the Pd−Cl distances of the approaching and leaving Cl are 2.839 and 2.738 Å, respectively. The resulting intermediate (M_6) has a tetraatomic cyclic structure that includes the palladium atom and the substrate chlorine atom now bridging the metal and one carbon atom. Then M_6 can transform into a new η^2 complex (M_7) by breaking the Cl−C bond in the four-membered cycle. M_7 is again a π intermediate which is 8.4 kcal mol^{-1} below the asymptotic limit. The $M_6 \rightarrow M_7$ energy barrier is very low: only 1.1 kcal mol^{-1}. The catalytic cycle is completed when a phosphine ligand enters the metal coordination sphere of M_7 and induces the expulsion of the acyl product. This final transformation, which restores the catalytic species (the *trans*-$Cl_2Pd(PH_3)_2$ complex), is characterized by a small barrier of 3.2 kcal mol^{-1} (transition state TS_8).

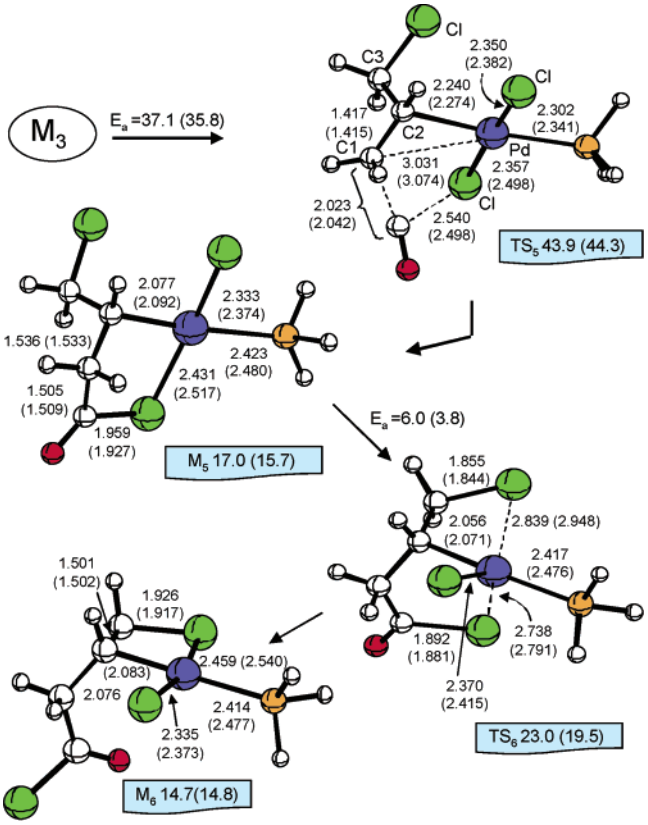

Figure 6. Schematic representation of the structures of TS_5, M_5, TS_6, and M_6. The energies (kcal mol^{-1}) are relative to noninteracting *trans*-$Cl_2Pd(PH_3)_2$ and allyl chloride (asymptotic limit). E_a = activation barriers. Values in parentheses: DZVP basis. Bond lengths are in angstroms and angles in degrees.

C. An Alternative Carbonylation Pathway: Direct Attack of Cl on the Palladium Atom (σ Pathway). We have demonstrated for both trans and *cis*-$Cl_2Pd(PH_3)_2$ the existence of an alternative carbonylation pathway involving a direct attack of the chlorine atom on the metal. We denote it as the σ pathway. The corresponding energy profiles are reported in Figure 8. Again, since the structures found along the channels originating from the trans and cis species (trans and cis channel, respectively) are very similar, we report in Figures 9 and 10 only those found along the lower energy path. These structures are discussed in detail, while

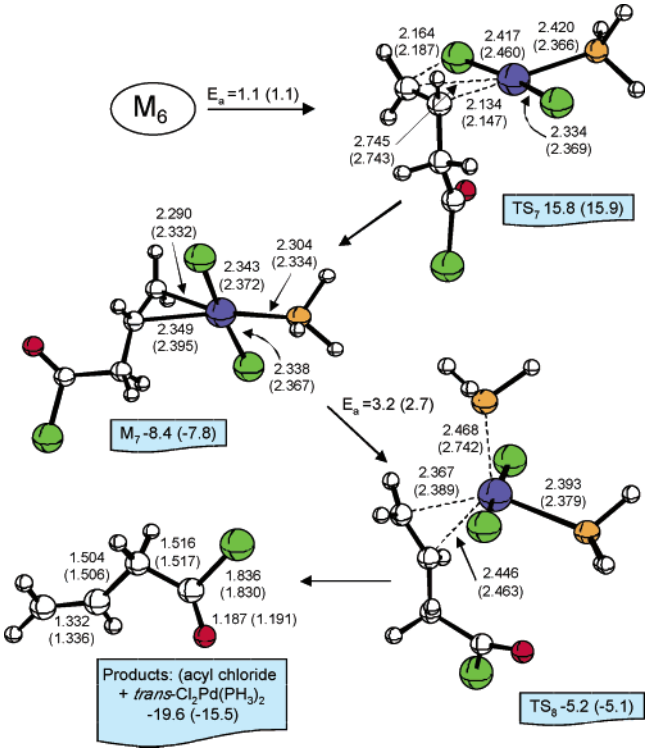

Figure 7. Schematic representation of the structures of TS_7, M_7, TS_8, and acyl chloride. The energies (kcal mol^{-1}) are relative to noninteracting *trans*-$Cl_2Pd(PH_3)_2$ and allyl chloride (asymptotic limit). E_a = activation barriers. Values in parentheses: DZVP basis. Bond lengths are in angstroms and angles in degrees.

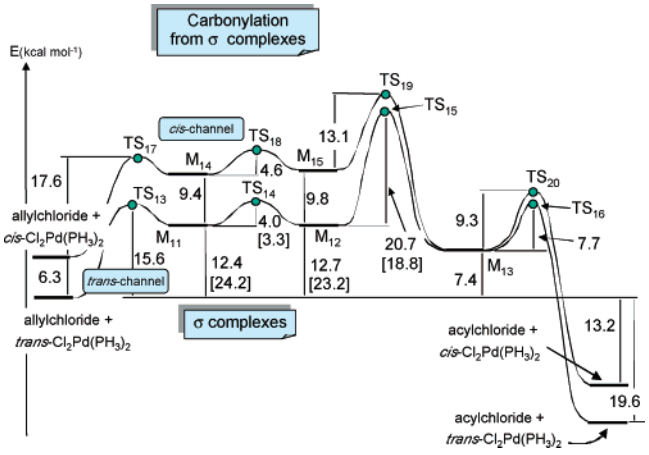

Figure 8. Energy profiles corresponding to the carbonylation from σ complexes (energy values in kcal mol^{-1}). Values in brackets include solvent effects (sdd/6-31G* basis).

the structures located along the cis channel are collected in the Supporting Information (Figures 3S and 4S).

The initial attack of Cl on the metal causes the expulsion of one PH_3 ligand and leads to the intermediate M_{11} (Figure 9), where the chlorine is now bridging one methylene carbon and the palladium (transition state TS_{13} with an energy barrier of 15.6 kcal mol^{-1}). The reaction is endothermic by 12.4 kcal mol^{-1}. The Cl−Pd bond of the bridge is 2.513 Å. Thus, as expected for a chlorine atom simultaneously involved in two bonds, it is significantly longer than the bonds of the other Cl ligands (2.327 and 2.347 Å). In M_{11} the

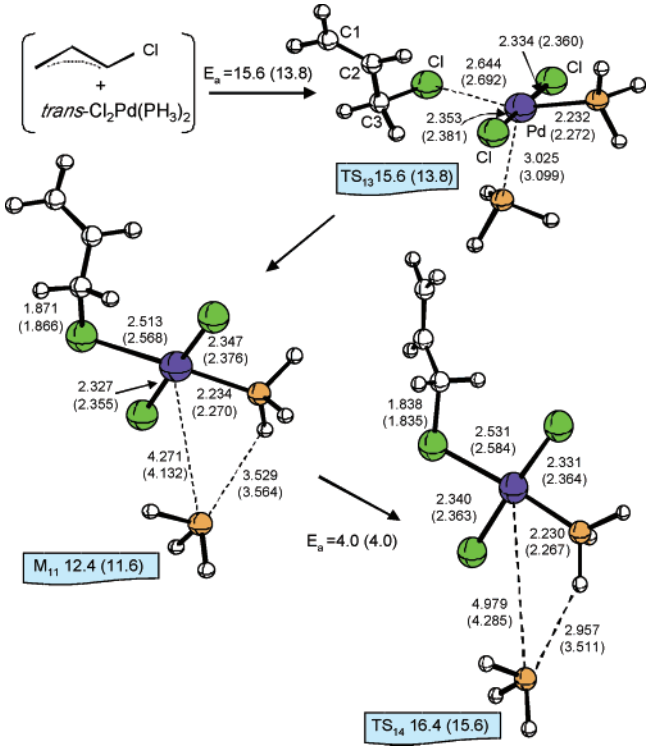

Figure 9. Schematic representation of the structures of TS_{13}, M_{11}, and TS_{14}. The energies (kcal mol^{-1}) are relative to noninteracting *trans*-$Cl_2Pd(PH_3)_2$ and allyl chloride (asymptotic limit). E_a = activation barriers. Values in parentheses: DZVP basis. Bond lengths are in angstroms and angles in degrees.

departing phosphine group is still weakly interacting with the metal (Pd−P distance 4.271 Å).

A conformational rearrangement (rotation around the C2−C3 bond) is now possible for M_{11} ($M_{11} \rightarrow M_{12}$ transformation). The rotation requires a barrier of 4.0 kcal mol^{-1} (transition state TS_{14} in Figure 9) and leads to a new intermediate (M_{12}) where the terminal methylene group is now oriented toward the metal. M_{12} is approximately degenerate with M_{11} (12.7 kcal mol^{-1} above the asymptotic limit).

A new transformation ($M_{12} \rightarrow M_{13}$) occurs when a CO molecule approaches M_{12}. The bent structure of this intermediate allows the carbon oxide to simultaneously interact with the metal and the free terminal methylene carbon of the substrate. This leads to a cyclic transition state (TS_{15}), where the C1−C(CO) and the Pd−C(CO) distances are 2.069 and 2.286 Å, respectively. Simultaneously, the C3−Cl bond of the bridge breaks and becomes 2.435 Å. The transformation requires overcoming a barrier of 20.7 kcal mol^{-1}. The resulting intermediate M_{13} has an octahedral structure (Figure 10) where the three chlorine atoms and one phosphine ligand are in equatorial positions, while the second PH_3 and the acyl product (σ bonded to the metal) are in axial positions.

A strong stabilization is obtained when the octahedral M_{13} intermediate transforms into the square-planar $Cl_2Pd(PH_3)_2$ complex and the product. This can occur along two different pathways (see Figure 11). In one case, the chlorine atom, which is opposite to the phosphine group, migrates from the metal to the carbonyl carbon. In the corresponding transition state TS_{16}, the

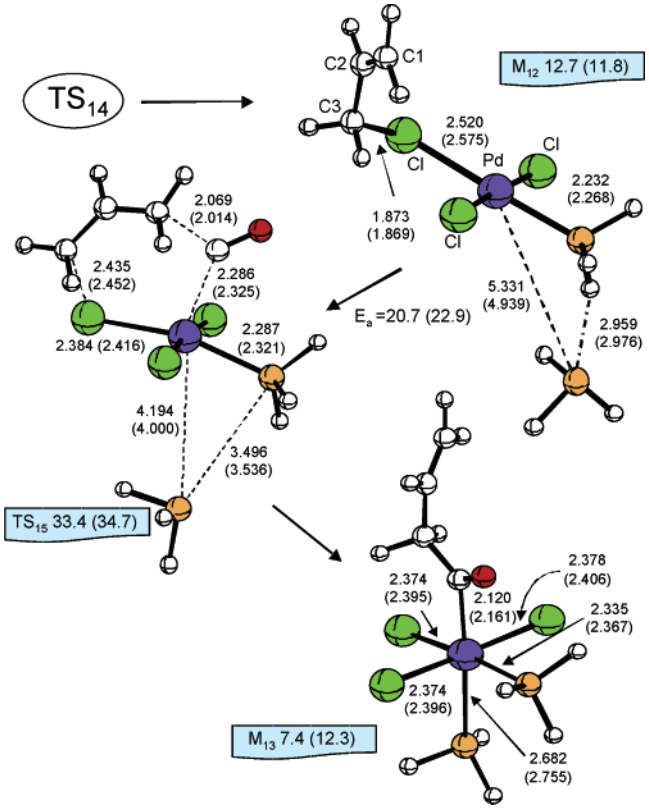

Figure 10. Schematic representation of the structures of M_{12}, TS_{15}, and M_{13}. The energies (kcal mol^{-1}) are relative to noninteracting *trans*-$Cl_2Pd(PH_3)_2$ and allyl chloride (asymptotic limit). E_a = activation barriers. Values in parentheses: DZVP basis. Bond lengths are in angstroms and angles in degrees.

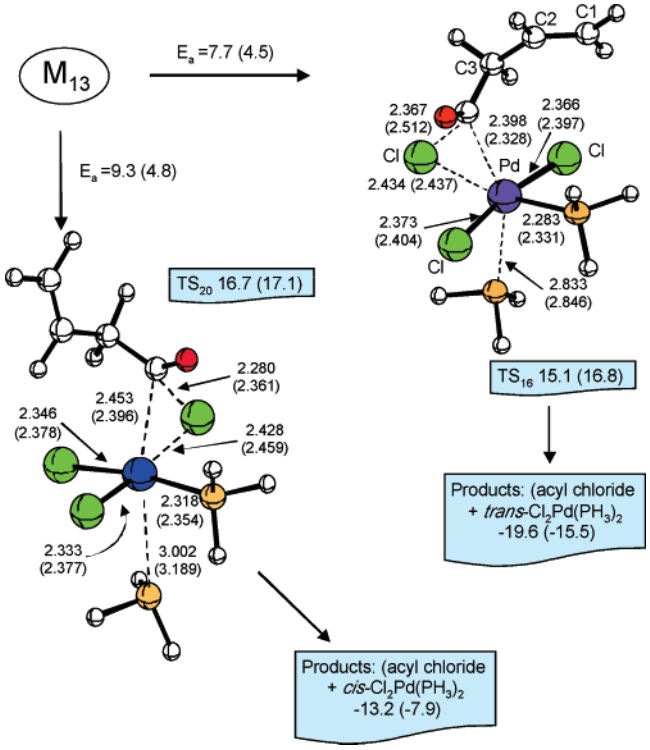

Figure 11. Schematic representation of the structures of TS_{16} and TS_{20}. The energies (kcal mol^{-1}) are relative to noninteracting *trans*-$Cl_2Pd(PH_3)_2$ and allyl chloride (asymptotic limit). E_a = activation barriers. Values in parentheses: DZVP basis. Bond lengths are in angstroms and angles in degrees.

chlorine is bridging the palladium and the carbon atoms (the Cl−Pd and Cl−C distances are 2.434 and 2.367 Å, respectively). This causes a weakening of the palladium−carbon bond, which becomes 2.398 Å (2.120 Å in M_{13}). By overcoming a barrier of 7.7 kcal mol^{-1}, this path leads to the final acyl chloride product and the regenerated catalyst in the form of the more stable *trans*-$Cl_2Pd(PH_3)_2$ complex. Along the second pathway the transition state TS_{20}, similar to TS_{16}, has been located. In this case one of the two chlorine atoms adjacent to PH_3 moves from the metal to the carbonyl carbon (the Cl−Pd and Cl−C(CO) distances are 2.428 and 2.280 Å, respectively) and causes the breaking of the Pd−C(CO) bond, which is 2.453 Å. This transformation, which has a barrier of 9.3 kcal mol^{-1}, leads to the acyl product and the less stable *cis*-$Cl_2Pd(PH_3)_2$ complex.

The σ pathway originating from the *cis*-$Cl_2Pd(PH_3)_2$ species (σ cis channel in Figure 8) is very similar to the σ trans channel (from *trans*-$Cl_2Pd(PH_3)_2$) and leads to the same intermediate, M_{13}. The two main barriers found in this case are 17.6 kcal mol^{-1} (attack of the chlorine and formation of the σ complex) and 13.1 kcal mol^{-1} (CO insertion). Figure 8 shows that the profile of the cis channel is always at higher energy than that of the trans channel. Consequently, the σ cis channel is highly disfavored.

It is important to note that the transition state highest in energy (TS_{15}) along the σ pathway originating from *trans*-$Cl_2Pd(PH_3)_2$ is 33.4 kcal mol^{-1} higher than the reactants, while the energy of TS_5 along the η^2 pathway is 43.9 kcal mol^{-1}. This indicates that the σ path is significantly favored with respect to that involving η^2 complexes and is discussed in the previous section.

D. Connection between the η^2 and σ Pathways. The η^2 complex M_3 (Figure 3) can be converted easily to the σ complex M_{12} (Figure 10) by overcoming a barrier of 13.3 kcal mol^{-1}. In the corresponding transition state TS_{21} (see Figure 12) the two Pd−C bonds, which characterize the η^2 interaction, are breaking (2.964 and 3.035 Å) and a bridging Cl−Pd bond is forming (2.863 Å). Notice that this is actually a η^3 complex, the only one that appears in our potential energy surface. TS_{21} represents a "gate" connecting the η^2 and σ pathways, and its existence suggests that, even if the carbonylation following the η^2 pathway is less likely than that occurring along the σ path, η^2 complexes can be involved in the overall process. In this case the reaction path could be as follows: (i) an η^2 pathway to reach M_1 and M_3; (ii) transformation from the η^2 complex M_3 to the σ complex M_{12}; (iii) carbonylation following the σ pathway, as discussed in part C. The three main barriers to be overcome would be 9.0 kcal mol^{-1} (transition state TS_1 for the transformation reactants → M_1), 13.3 kcal mol^{-1} ($\eta^2 \rightarrow \sigma$ transformation), and 20.7 kcal mol^{-1} (transition state TS_{15} for the transformation $M_{12} \rightarrow M_{13}$). Thus, this $\eta^2 + \sigma$ pathway to carbonylation can effectively compete to form the final acyl product.

E. Fate of the $Cl_2Pd(CO)PH_3$ Species. To understand the role of $Cl_2Pd(CO)PH_3$ as the active species, we have investigated the process affording this complex and we have considered its interaction with a substrate

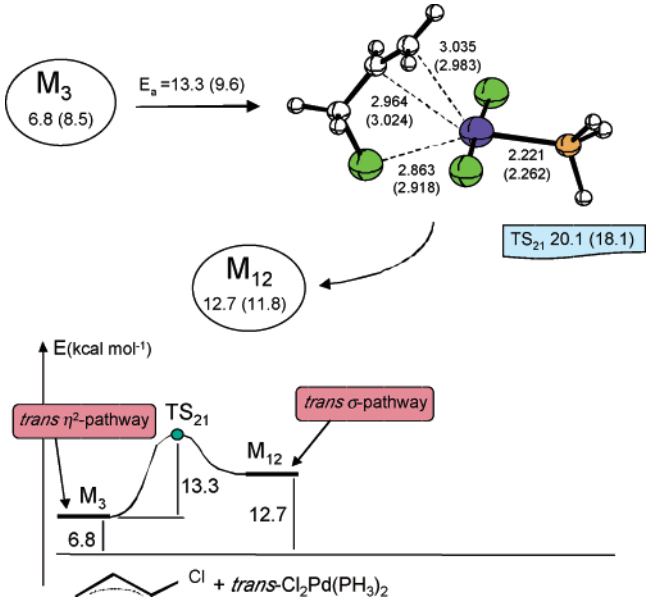

Figure 12. Schematic representation of the structure of TS_{21} corresponding to the gate between the η^2 and σ pathway. The energies (kcal mol^{-1}) are relative to noninteracting *trans*-$Cl_2Pd(PH_3)_2$ and allyl chloride (asymptotic limit). E_a = activation barriers. Values in parentheses: DZVP basis. Bond lengths are in angstroms and angles in degrees.

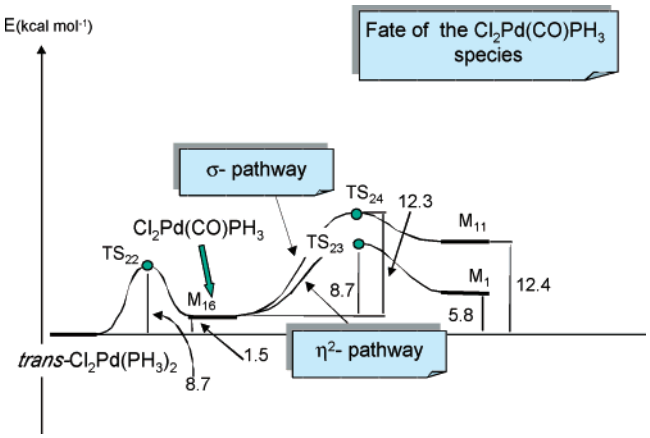

Figure 13. Energy profiles describing the fate of the $Cl_2Pd(PH_3)_2$ species (energy values in kcal mol^{-1}).

molecule either along a η^2 or a σ pathway. The energy profiles are represented in Figure 13 and the corresponding structures are reported in Figure 14.

The formation of *trans*-$Cl_2Pd(CO)PH_3$ (M_{16} along the energy profile) from the *trans*-$Cl_2Pd(PH_3)_2$ complex is endothermic by 1.5 kcal mol^{-1} and requires overcoming a barrier of 8.7 kcal mol^{-1}. In the corresponding transition state (TS_{22}) a CO molecule enters the metal coordination sphere and causes the simultaneous expulsion of one phosphine ligand (the Pd−P and Pd−C(CO) distances are 2.512 and 2.142 Å, respectively, and the ∠CPdP angle is 107.8°). Two reaction channels originating from M_{16} have been identified. In one case the π-allyl system directly attacks the metal (η^2 pathway) with an activation barrier of 8.7 kcal mol^{-1} (transition state TS_{23}), leading to the η^2 complex M_1 of Figure 2. In the other case (σ pathway), a direct attack of the chlorine on the metal is observed. It requires a higher activation energy (12.3 kcal mol^{-1} for transition state

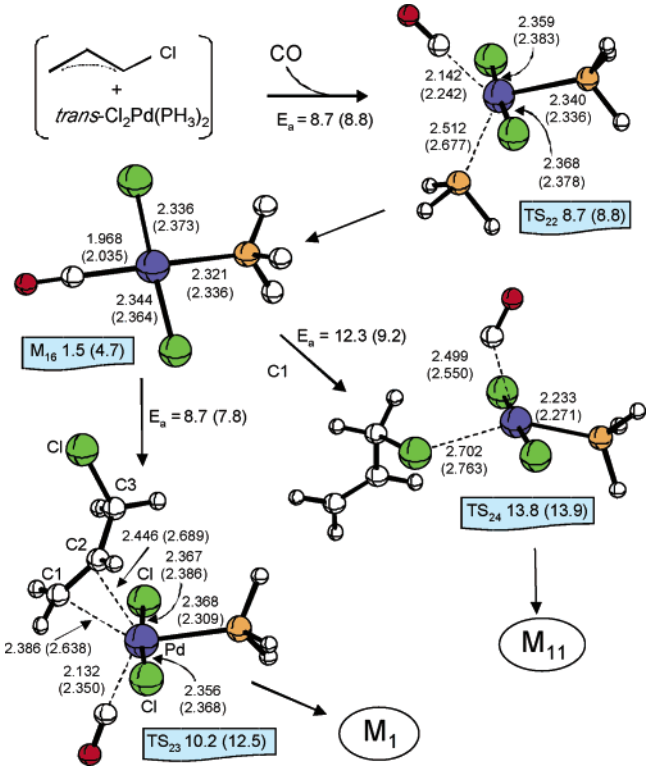

Figure 14. Schematic representation of the structures of TS_{22}, M_{16}, TS_{23}, and TS_{24}. The energies (kcal mol^{-1}) are relative to noninteracting *trans*-$Cl_2Pd(PH_3)_2$ and allyl chloride (asymptotic limit). E_a = activation barriers. Values in parentheses: DZVP basis. Bond lengths are in angstroms and angles in degrees.

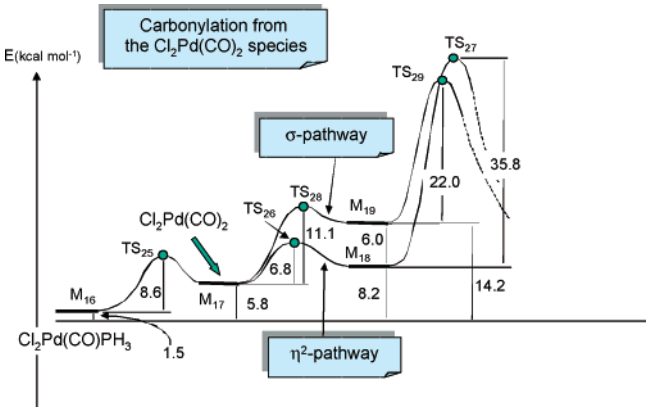

Figure 15. Energy profiles corresponding to the carbonylation from the $Cl_2Pd(CO)_2$ species along the η^2 and σ pathways (energy values in kcal mol^{-1}).

TS_{24}) and points to the intermediate complex M_{11} already depicted in Figure 8. Thus, the reaction of the substrate with *trans*-$Cl_2Pd(CO)PH_3$ leads the system to the same η^2 and σ reaction channels already discussed for the catalysis operated by *trans*-$Cl_2Pd(PH_3)_2$ (see the previous sections).

F. $Cl_2Pd(CO)_2$ as Active Species: Does a Carbonylation Pathway Originating from This Complex Exist? An additional CO attacking the $Cl_2Pd(CO)PH_3$ complex can cause the expulsion of the second phosphine ligand to afford the $Cl_2Pd(CO)_2$ species, which, in principle, can be active in the carbonylation (see Figure 15). A barrier of 8.6 kcal mol^{-1} (transition state TS_{25}; see Figure 16) must be overcome

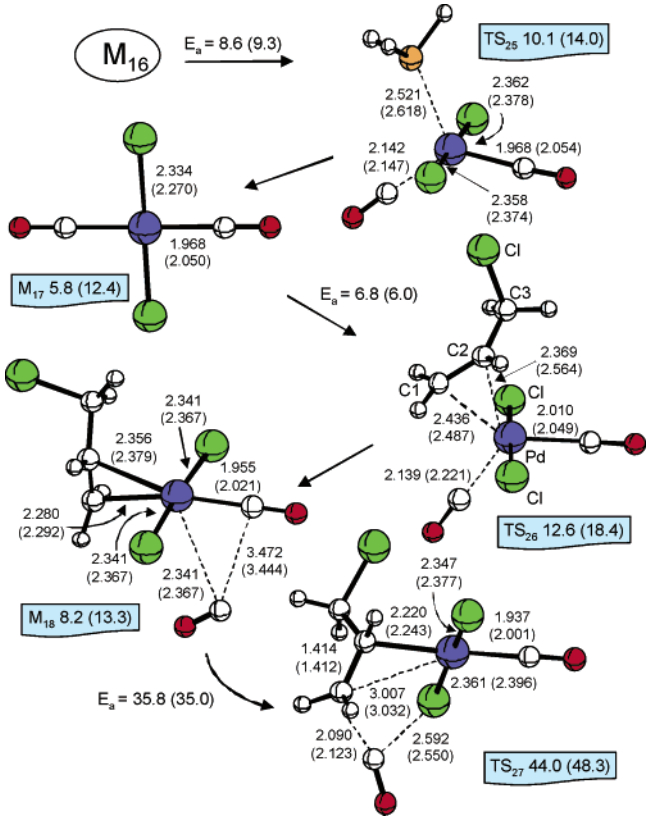

Figure 16. Schematic representation of the structures of TS_{25}, M_{17}, TS_{26}, M_{18}, and TS_{27}. The energies (kcal mol^{-1}) are relative to noninteracting *trans*-$Cl_2Pd(PH_3)_2$ and allyl chloride (asymptotic limit). E_a = activation barriers. Values in parentheses: DZVP basis. Bond lengths are in angstroms and angles in degrees.

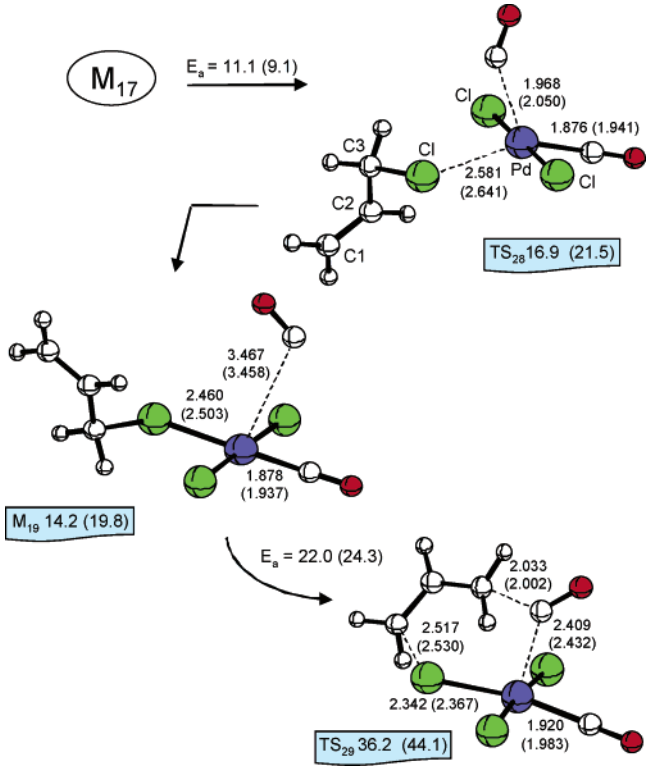

Figure 17. Schematic representation of the structures of TS_{28}, M_{19}, and TS_{29}. The energies (kcal mol^{-1}) are relative to noninteracting *trans*-$Cl_2Pd(PH_3)_2$ and allyl chloride (asymptotic limit). E_a = activation barriers. Values in parentheses: DZVP basis. Bond lengths are in angstroms and angles in degrees.

to form $Cl_2Pd(CO)_2$. This complex (M_{17}; see Figure 16) is 5.8 kcal mol^{-1} higher in energy than the starting $Cl_2Pd(PH_3)_2$ species and 4.3 kcal mol^{-1} higher than $Cl_2Pd(CO)PH_3$. Thus, the equilibrium $Cl_2Pd(PH_3)_2 + 2CO = Cl_2Pd(CO)PH_3 + CO + PH_3 = Cl_2Pd(CO)_2 + 2PH_3$ is shifted to the left and only a small amount of $Cl_2Pd(CO)_2$ will be present at low CO pressure. However, the number of $Cl_2Pd(CO)_2$ molecules can significantly increase if high CO pressures are used. Consequently, we have also investigated the existence of η^2 and σ pathways involving $Cl_2Pd(CO)_2$ as a catalyst. The corresponding reaction profiles, originating from M_{17}, are shown in Figure 15. The structures of the corresponding critical points are depicted in Figures 16 and 17.

A small barrier of 6.8 kcal mol^{-1} (transition state TS_{26}) is needed to form the η^2 intermediate M_{18}. The structure of M_{18} (Figure 16), where the substrate π system interacts with the palladium atom, is very similar to that of M_1 (reported in Figure 3). The small differences observed in the metal−ligand bond lengths are determined by the CO ligand that replaces the PH_3 group in the position opposite to the substrate and by the expelled CO that still weakly interacts with the metal (Pd−C(CO) distance 2.341 Å). The structural features of the critical points that follow along the pathway leading to the final product are expected to be similar to those found on the η^2 pathway that originates from $Cl_2Pd(PH_3)_2$. In agreement with this similarity a transition state (TS_{27}), almost identical with TS_5, has been located. Since the corresponding activation energy is 35.8 kcal mol^{-1} (it was 37.1 kcal mol^{-1} for TS_5), this transition state, which represents the kinetically important step, is 44.0 kcal mol^{-1} above the asymptotic limit (reactants $Cl_2Pd(PH_3)_2$ + allyl chloride).

The direct σ attack of Cl on the metal (transition state TS_{28}, Figure 17) has a barrier of 11.1 kcal mol^{-1} and induces the removal of a CO ligand from $Cl_2Pd(CO)_2$. In the resulting intermediate (M_{19}) the expelled CO is still weakly interacting with the metal (Pd−C(CO) distance 3.467 Å). M_{19}, which is 14.2 kcal mol^{-1} above the asymptotic limit (6.0 kcal mol^{-1} above M_{18}), strongly resembles M_{11} found along the σ pathway (see section C). The transition state TS_{29}, similar to TS_{15}, describes the formation of the acyl fragment. The CO unit again forms a bridge between the metal and one methylene, and the chlorine atom simultaneously moves from the substrate to the metal. Since this step has a barrier of 22.0 kcal mol^{-1} (it is the rate-determining step along this reaction path), TS_{27} lies 36.2 kcal mol^{-1} above the reactants and only 2.8 kcal mol^{-1} above TS_{15}. These results suggest that, in the presence of high CO pressure, this way to carbonylation could become important.

G. Solvent Effect. The energy values of the most important critical points have been re-computed in the presence of the solvent effects with the sdd/6-31G* basis and are reported in square brackets in Figures 2, 5, 8, and 15. The emulated solvent is CH_2Cl_2 (dielectric constant $\epsilon = 8.93$), one of the solvents commonly used in the experiment. In all cases we have found that, after solvating the system, the energy difference of the various structures with respect to reactants significantly

increases. However, this does not remarkably affect the various activation barriers (E_a) that determine the overall mechanistic picture. For instance, along the η^2 pathway, for the two transformations $M_1 \rightarrow TS_3 \rightarrow M_3$ and $M_3 \rightarrow TS_5 \rightarrow M_5$ we have found 2.7 and 36.2 kcal mol^{-1}, respectively (3.0 and 37.1 kcal mol^{-1} in the gas phase). Similarly, along the σ pathway the barrier for the transformation $M_{12} \rightarrow TS_{15} \rightarrow M_{13}$ becomes 18.8 kcal mol^{-1} (20. 7 kcal mol^{-1} in the gas phase). Consequently, the difference between TS_5 and TS_{15} is now 8.1 kcal mol^{-1} and the σ pathway is still highly favored. Thus, the inclusion of the solvent effects in the computations does not affect the mechanistic scenario obtained with the simple gas-phase model.

H. Basis Set Effect. To test the reliability of the less accurate DZVP basis set, we have reoptimized at this level of accuracy all the critical points previously discussed. This point is rather important, since the use of the DZVP basis can significantly increase the computational expedience and allow the investigation of larger systems.

The DZVP energy values and geometrical parameters are reported in parentheses in the figures. For instance, if we consider again the two transformations $M_1 \rightarrow TS_3 \rightarrow M_3$ and $M_3 \rightarrow TS_5 \rightarrow M_5$ along the η^2 pathway, we have found with the smaller basis 2.9 and 35.8 kcal mol^{-1}, respectively (3.0 and 37.1 kcal mol^{-1} with the sdd/6-31G* basis). The transformation $M_{12} \rightarrow TS_{15} \rightarrow M_{13}$ along the σ pathway has now a barrier of 22.9 kcal mol^{-1}, which must be compared to 20.7 kcal mol^{-1} obtained with the sdd/6-31G* basis. Thus, the difference between TS_5 and TS_{15} is now 9.6 kcal mol^{-1} and the σ pathway is still the most likely path, as indicated in the previous sections. Inspection of the various structures reported in the figures show that also the geometrical parameters obtained at the two levels of accuracy are very similar.

Conclusions

In this paper we have carried out a theoretical study at the DFT(B3LYP) level on the carbonylation reaction of allyl halides catalyzed by palladium complexes. We have considered a model system formed by an allyl chloride molecule reacting with CO in the presence of $Cl_2Pd(PH_3)_2$. This system emulates the case of a Pd(II) species acting as a catalyst. The most important results can be summarized as follows.

(i) We have demonstrated the existence of two different reaction pathways leading to the carbonylation product (β,γ-unsaturated acyl chloride). In one case (η^2 pathway) the carbonylation proceeds via the formation of a π-allyl palladium intermediate. In the other case (σ pathway) the process involves a direct attack of the chlorine on the metal.

(ii) The π-allyl palladium intermediate is a η^2 complex. No evidence for the existence of a η^3 complex intermediate has been found.

(iii) The carbonylation along the η^2 pathway occurs via a rather complex mechanism, where the CO unit does not insert directly into a Pd−C bond. Instead, the CO interacts simultaneously with one of the two Cl ligands and the closest double-bond carbon, leading to a cyclic structure where the acyl chloride group is already formed. This structure transforms to a new η^2 π complex between the palladium and the β,γ-unsaturated acyl chloride. The main activation barrier found along this path is 35.4 kcal mol^{-1}, and the corresponding transition state is 43.9 kcal mol^{-1} above the asymptotic limit.

(iv) The direct attack of the chlorine on the metal (σ pathway) requires the overcoming of two main barriers of 15.6 and 20.7 kcal mol^{-1}. Since the transition state highest in energy is 33.4 kcal mol^{-1} above the asymptotic limit, this path is definitely favored with respect to that involving π complexes. Along the σ pathway we have located an octahedral intermediate, an unusual coordination state for a palladium complex. In this intermediate the acyl product is σ-bonded to the metal.

(v) A "gate" on the potential surface joins the η^2 and σ pathways. This allows the transformation of the η^2 complexes to the σ complexes immediately preceding the CO insertion. This "gate" between the two channels (i.e. formation of the η^2 complex followed by the transformation to the σ complex) represents an alternative route to afford the carbonylation product, avoiding the high activation barrier encountered along the η^2 path. Thus, the role of the substrate allyl system is that of providing an additional reaction channel that uses the $\eta^2 \rightarrow \sigma$ "gate" to access the main reaction σ pathway (the direct coordination of the chlorine to the metal). Clearly, this is not feasible for a saturated halide, where the only way to carbonylation remains the σ pathway. The existence of the $\eta^2 \rightarrow \sigma$ connection can also explain the experimental evidence that points to a π complex as the likely intermediate of the carbonylation reaction.

(vi) The *trans*-$Cl_2Pd(CO)PH_3$ complex, which originates from the reaction of *trans*-$Cl_2Pd(PH_3)_2$ with CO, is also a possible catalytic species. However, the η^2 and σ paths that originate from this species, meet immediately the main η^2 and σ reactions channels previously discussed.

(vii) A third possible catalytic species is represented by $Cl_2Pd(CO)_2$, which forms from the reaction of $Cl_2Pd(CO)PH_3$ with CO. For $Cl_2Pd(CO)_2$, both η^2 and σ reaction pathways exist and the σ one is again favored. Our data indicate that this way to carbonylation can become important when high CO pressure (and consequently high concentration) are used. This point is important in light of the fact that high CO pressures are one of the most common working conditions required by palladium-catalyzed carbonylation reactions.

(viii) It is important to stress that the existence of the σ path as the most likely route to carbonylation seems to be a common feature for these reactions. A similar path was demonstrated to exist for the carbonylation of allyl halides catalyzed by nickel carbonyl $Ni(CO)_4$.[17]

(ix) It is interesting to outline that the activation barriers computed for the nickel-catalyzed carbonylation of allyl halides[17] are significantly lower than those obtained here for the palladium-catalyzed process. This is in agreement with the fact that, while mild reaction conditions are required in the former case, significantly stronger conditions (high temperature and pressure) must be used in the latter.

(vii) The inclusion of the solvent effects in the computations (CH_2Cl_2 is emulated) does not remarkably change the activation barriers of the rate-determining

steps and does not affect the mechanistic scenario obtained with the simple gas-phase model.

Acknowledgment. M.A.C. and J.J.N. acknowledge the Spanish "Ministerio de Ciencia y Tecnología" and the Catalan "CIRIT" for grants (Nos. BQU2002-04587-C02-02 and 2001SGR-0044, respectively) and also the CEPBA-IBM Research Institute, CEPBA, and CESCA for the allocation of CPU time on their computers. M.A.C. also thanks the University of Barcelona for a Ph.D. grant. G.P.M. and A.B. acknowledge the CNR and MIUR for the grant COFIN 2003: "Stereoselective reactions promoted by new catalytic systems: synthesis and modeling".

Supporting Information Available: Figures 1S−4S, giving additional schematic representations of species discussed in the paper. This material is available free of charge via the Internet at http://pubs.acs.org.

OM049301Y